The Effects of Damkohler Number on a Turbulent Shear Layer - Experimental Results

by

M. G. Mungal and C. E. Frieler

31 December 1985

GALCIT Report FM85-01

Graduate Aeronautical Laboratories

California Institute of Technology

Pasadena, CA 91125

The Effects of Damkohler Number on a Turbulent Shear Layer - Experimental Results

M. G. Mungal and C. E. Frieler

ABSTRACT

A chemical reaction for which the reaction rate can be varied is studied in a fully developed, two-dimensional, turbulent mixing layer. The layer is formed between two nitrogen streams, one carrying low concentrations of fluorine and the other hydrogen and nitric oxide. For fixed concentrations of fluorine and hydrogen and for nitric oxide concentrations that are small fractions of the fluorine concentration, the heat release is fixed but the overall reaction rate is controlled by the nitric oxide concentration. Therefore, for fixed flow conditions, the nitric oxide concentration determines the ratio of the reaction rate to the mixing rate. For large values of this ratio, the amount of product, at a given downstream location, measured by the mean temperature rise, is independent of the reaction rate, i.e., the reaction is mixing limited. As the reaction rate is reduced the major effects are: (1) amount of product declines (as expected), (2) the mean temperature profile, which is initially somewhat unsymmetrical because the hydrogen-fluorine freestream concentration ratio is set at a large value, becomes symmetrical, and (3) the ramp-like instantaneous temperature traces within the large structure gradually become more top-hat.

The Effects of Damkohler Number on a Turbulent Shear Layer - Experimental Results

M. G. Mungal and C. E. Frieler

1. Introduction

This work represents the third in a series of studies aimed at achieving an understanding of mixing and combustion in a fully developed, two-dimensional, turbulent mixing layer, Fig. 1. In these experiments, the reactants are low concentrations of hydrogen and fluorine carried in separate nitrogen freestreams. Nitric oxide, in concentrations that are small compared to the fluorine, is carried with the hydrogen stream. When the two streams mix, the nitric oxide dissociates a fraction of the fluorine to initiate and control the hydrogen-fluorine chain reaction. In all experiments, the heat release is sufficiently low that the heat release does not couple with the fluid mechanics, so that the overall properties of the mixing layer are not significantly changed from those of the non-reacting case. It is important to note that the present chemical system is hypergolic (low activation energy) at all concentrations, unlike hydrocarbon - air systems which require ignition sources to sustain combustion, have flammability limits and can be quenched by high values of strain rate.

The first of these efforts [1,2] examined the effects of the hydrogen-fluorine freestream concentration ratio upon the amount of product formed in the fully developed layer at a single Reynolds number of $\sim 4\times10^5$ (based on velocity difference and downstream distance). The results confirmed the central role of the large structure dynamics in mixing and combustion. The asymmetry in entrainment of the mixing layer was demonstrated through 'flip' experiments whereby the lean reactant being

carried on the high-speed or low-speed side of the layer leads to different amounts of product. The experiments also showed that when one reactant concentration is fixed, a nearly asymptotic product profile is reached when the other reactant concentration is approximately eight times the first. Under these conditions, essentially all the molecularly mixed lean reactant is completely consumed. It is instructive to note that for chemical reactions in water at similar Reynolds numbers, Koochesfahani [3] found that there was approximately 50% less (normalized) product than in the gas. This has led to the conclusion that the Schmidt number influences the amount of product formed in turbulent flows, even at Reynolds numbers as high as 4×10^5.

In the second effort [4], the dependence of the amount of product formed in the mixing layer upon Reynolds number was studied. It was found that the large organized structures are present at all Reynolds numbers investigated, irrespective of whether the boundary layer on the splitter plate is laminar or turbulent, and that the product dependence on Reynolds number is weak. There is, approximately, a 20% decrease in the amount of product formed for a factor of 10 increase in Reynolds number (or 6% decrease per factor of 2 in Reynolds number).

In both of the above investigations, the amount of nitric oxide was sufficiently large to insure that the reaction was, to a good approximation, mixing limited. In the present investigation we reduce the nitric oxide concentration to study the effects of the chemical reaction rate. A chemical kinetics code, CHEMKIN [5], was used to study the hydrogen-fluorine-nitric oxide system. The results show that the nitric oxide concentration controls the overall reaction rate, while the heat of reaction is the same. Since the runs described below are all performed at low heat, the fluid mechanics also remains unchanged.

In the investigations mentioned above, the findings were interpreted in the context of the simple model for mixing and product formation in the turbulent shear layer proposed by Broadwell & Breidenthal [6]. The

present results are interpreted in terms of this model in Broadwell & Mungal [7].

2. The Chemical Reactions

The principal reactions in the experiment consists of the hydrogen-fluorine chain reaction and the nitric oxide fluorine dissociation reaction.

$$H_2 + F \xrightarrow{k_1} HF + H, \quad \Delta Q = -32 \frac{kcal}{mole}, \quad \underline{k}_1 = 2.6\times10^{12}\underline{T}^{0.5}\exp(\frac{-610}{\underline{RT}}) \qquad (1)$$

$$H + F_2 \xrightarrow{k_2} HF + F, \quad \Delta Q = -98 \frac{kcal}{mole}, \quad \underline{k}_2 = 3\times10^{9}\underline{T}^{1.5}\exp(\frac{-1680}{\underline{RT}}) \qquad (2)$$

$$NO + F_2 \xrightarrow{k_3} NOF + F, \quad \Delta Q = -18 \frac{kcal}{mole}, \quad \underline{k}_3 = 4.2\times10^{11}\exp(\frac{-2285}{\underline{RT}}) \qquad (3)$$

where k is given in cc/mole-s, T in degrees K and R is the universal gas constant in cal/mole-K.

Reactions (1) and (2) are the so-called cold and hot reactions, respectively. The cold reaction, which carries 25% of the total heat release, is faster than the hot reaction by about an order of magnitude at 300K ($k_1 \simeq 1.6\times10^{13}$, $k_2 \simeq 9.5\times10^{11}$). The rate constants k_1 and k_2 are taken from Cohen & Bott [8] and k_3 from Baulch et al. [9].

Additional reactions which must be considered are:

$$F + NO + M \xrightarrow{k_4} NOF + M, \quad \Delta Q = -57 \frac{kcal}{mole}, \quad \underline{k}_4 \simeq 3\times10^{16} \qquad (4)$$

and

$$F + F + M \xrightarrow{k_5} F_2 + M, \qquad k_5 \simeq 3.2\times10^{14} \tag{5}$$

$$H + F + M \xrightarrow{k_6} HF + M, \qquad k_6 \simeq 2.5\times10^{16} \tag{6}$$

$$H + H + M \xrightarrow{k_7} H_2 + M, \qquad k_7 \simeq 3.0\times10^{15} \tag{7}$$

where the k_4 - k_7 rates are given in $cc^2/mole^2$-s and are estimated at 300K from Baulch et al. [9].

We have used the CHEMKIN [5] computer code to study the reaction set (1) - (7) in a premixed constant pressure reactor. The initial condition 4%H_2, 0.5%F_2, 0.015%NO in a N_2 diluent simulate our normal operating conditions of 8%H_2, 0.03%NO in N_2 on the high-speed side and 1%F_2 in N_2 on the low-speed side (this nominal condition will be referred to as $[NO]^*$). The CHEMKIN code computes the species concentration and temperature as a function of time for the mixture at constant pressure or constant volume, the former being the option applicable to this work. The result of such a calculation is shown in Fig. 2. The starting temperature is 300K and the system asymptotes to a temperature of 393K. The figure shows the results if only the first three reactions (1)-(3) are used, together with that for all seven reactions (1)-(7). The agreement suggests that reactions (1)-(3) determine the behaviour of the chemical system at these temperatures, while (4)-(7) are relatively less important. We have fitted a straight line to the curve shown in Fig. 2 and taken the time required for a temperature rise from 300K to 393K to be a measure of the chemical time of the system. Fig. 2 shows that for the rate constants shown above, the chemical time for our nominal condition, τ^*, is 0.53 ms. (It is worthwhile to note that if we simulate an operating condition of 1%K_2, 0.03% NO together with 1%F_2 in a N_2 diluent, as was performed in Reference 2, the chemical time increases by about 15%.)

Table 1 shows (among other results) the overall chemical rate, k (the inverse of the chemical time, τ) as computed by CHEMKIN, for various concentrations of nitric oxide for the reaction set (1)-(7). As is shown

analytically in Appendix 1, the chemical rate is nearly proportional to [NO] at very low concentrations (relative to $[F_2]$) and varies as the square root of [NO] at higher concentrations. In summary, the chemical system (1)-(7) describes, for our conditions, a reaction in which the heat release is fixed by the hydrogen and fluorine concentrations but the overall rate is controlled by the nitric oxide concentration.

3. Experimental Apparatus

The experimental facility has been described previously [1,2] and will only be discussed briefly here. It is of the blowdown type in which premixed volumes of hydrogen and nitric oxide in nitrogen, and fluorine in nitrogen are discharged through sonic orifices, maintaining a constant mass flux in each of the freestreams. Both streams enter a settling and contraction section for turbulence reduction with the high speed flow emerging from a 6:1 contraction at an exit area of 5 x 20 cm, and the low speed emerging from a 4:1 contraction in a 7.5 x 20 cm exit area. The flows then meet at the tip of a splitter plate as shown in Fig. 1. All measurements are recorded at a station x = 45.7 cm downstream of the splitter plate trailing edge.

Runs were performed for flow velocities of U_1 = 22 and 44 m/s with a fixed speed ratio U_2/U_1 = 0.40. The Reynolds numbers based on the velocity difference ΔU, and the 1% thickness of the layer δ_1 (distance between points at which the mean temperature rise is 1% of the maximum mean temperature rise), and the cold kinematic viscosity of nitrogen are respectively 6.7×10^4, and 1.3×10^5. These values are all beyond the mixing transition observed by Konrad [10] and Breidenthal [11]. The high speed turbulence level is about 0.7% rms at the lower speed and decreases somewhat at the higher speed. For U_1 = 22 m/s, the high-speed boundary layer momentum thickness, θ_1, was estimated using Thwaites' method, with the Reynolds number $U_1\theta_1/\nu$ estimated to be 240. Thus at the measuring station, $x/\theta_1 \simeq 2800$.

4. Measurements

For each run, the streamwise pressure gradient is set to zero by adjustment of the low speed sidewall. Temperature rise is recorded by a rake of 8 cold wire resistance thermometers placed across the width of the layer, each driven by a constant current of 0.4mA. The wires are made of 2.5 μm diameter platinum / 10% rhodium welded to inconel prongs with a span of 1.5 mm. The ratio of the length of the wire to Betchov's cold length [12] is about 20 at the lower Reynolds number. During a run, each wire is sampled at 10 and 12.5 kHz for the two speeds, corresponding to total data rates of 80 and 100 kHz.

As described in [2], the cold wires are calibrated directly before each run and record an accurate mean temperature profile, while excursions from the mean suffer from conduction error due to the prongs and the thermal lag of the wire itself [13], [14]. The mean temperature profiles were spot checked by a 0.25 mm diameter chromel-alumel thermocouple at a single point on the mean temperature rise profile, with the agreement being generally within 3% or better. The mean temperature profiles shown below are repeatable from run to run to within 2 percent. The absolute reactant concentrations however, are known only to approximately 3-5%, and thus the absolute value of the potential heat release has an uncertainty of the same order.

5. Experimental Results and Discussion

For the runs reported here, the high-speed stream consisted of 8%H_2, 92%N_2 together with varying small concentrations of NO, while the low-speed stream consisted of 0.96%F_2 and 99%N_2 (passivation of upstream screens and plates removed an estimated 0.04%F_2 from the nominal value of 1%F_2), with an adiabatic flame temperature rise of 159K. As was noted above, this choice of reactant concentrations guarantees that, when the reaction rate is sufficiently high, the fluorine (lean reactant) which is

molecularly mixed with the hydrogen is almost totally consumed.

Figure 3a shows the mean temperature rise profiles obtained at the $x - x_0 = 45.7$ cm station for the cases of decreasing nitric oxide concentration, namely $[NO]/[NO]^* = 1, 1/2, 1/4, 1/8, 1/16, 1/23, 1/32, 0$ at $U_1 = 22$ m/s (note that the accuracy in loading our nominal concentration of NO is probably within 3% but becomes progressively worse as the amount of NO decreases). The symbols indicate the measured average temperature rise at the positions of the eight probes, and represents the average of 12,288 points per probe during which time at least 100 structures would have passed the measuring station. The smooth curve is an exponential fit of the type

$$\bar{T}(\eta)/Tflm = \exp (c_0 + c_1\eta + c_2\eta^2 + c_3\eta^3 + c_4\eta^4)$$

where T is the local mean temperature rise, Tflm is the adiabatic flame temperature rise, $\eta \equiv y/(x-x_0)$, and the point $\eta = 0$ corresponds to the position of the dividing streamline (see Table 3).

We see that, as [NO] decreases, there is a gradual loss in area under each of the product profiles, together with a tendency for the profile to become more symmetric. In fact, for the case $[NO]/[NO]^* = 1/32$, the profile is remarkably symmetric in spite of the fact that the high-speed reactant is eight times more concentrated than the low-speed reactant. This trend towards symmetry is shown more directly in Fig. 3b where all profiles have been scaled to the same height and Fig. 3c where the cases $[NO]/[NO]^* = 1, 1/32$ are shown. It should also be noted that the case $[NO]/[NO]^* = 0$ shows no product both experimentally and in computation with the CHEMKIN code.

Figure 4 shows the mean temperature rise profiles for the cases of increasing the nitric oxide concentration, namely $[NO]/[NO]^* = 1, 3/2, 2$. Table 1 indicates that the effective reaction rates for the latter two runs are larger than the nominal by factors of 1.3 and 1.5 respectively.

The similarity of the profiles implies that the reaction is mixing rate limited for [NO] at the nominal value and above.

Figure 5a shows similar results taken at the same measuring station, but with U_1 = 44 m/s (and $U_2 = 0.4U_1$ to maintain the same speed ratio) for the cases $[NO]/[NO]^*$ = 2, 1, 1/4, 1/16 (see also Table 2,4). The scaled profiles for the cases $[NO]/[NO]^*$ = 1, 1/16 are shown in Fig. 5b to again demonstrate the symmetrizing of the mean temperature profile. It is worthwhile to note that, in the fast chemistry limit, the absolute area under the temperature profile for the U_1 = 44 m/s case is less, by about 10 percent, than that for U_1 = 22 m/s. As is discussed in [4], this is believed to be a Reynolds number effect and not a Damkohler number effect, since increasing the [NO] concentration by a factor of 2 at both Reynolds numbers with the corresponding increase in chemical rates, does not eliminate the difference.

The amount of product generated by the reaction is characterized by the product thickness

$$\delta_p \equiv \int_{-\infty}^{\infty} \frac{c_p(y)}{c_\infty}\, dy = \int_{-\infty}^{\infty} \frac{C_p\, \bar{T}(y)}{c_\infty\, \Delta Q}\, dy$$

where $c_p(y)$ is the concentration of product and c_∞ is the freestream fluorine concentration. Since product is analogous to temperature rise, the second expression is obtained by making use of the mean temperature rise profile $\bar{T}(y)$, the molar heat capacity of the carrier gas, C_p, and the heat release per mole of reactant, ΔQ. The product thickness of the curves of Figs. 3a, 4 normalized by the 1% thickness is shown in Fig. 6a as a function of the nitric oxide concentration. For small values of [NO], there is a rapid increase in the amount of product with the kinetic rate in what could be called the 'slow-chemistry' regime. At the larger values of [NO], the product amount is nearly independent of [NO] implying that the reaction is mixing limited, i.e. that the chemical rate is fast relative to the mixing rate. Also shown in Fig. 6 are the results for the

U_1 = 44 m/s case. The same data are shown in Fig. 6b as a function of the Damkohler number, Da (defined as the ratio of the mixing time to the chemical time). We have chosen the time of flight at the mean convection speed $(U_1+U_2)/2$ from the mixing transition, x_t, to the measuring station, x, to be an appropriate measure of the mixing time (see Broadwell &Mungal [7]). The CHEMKIN results are used for the chemical time. This choice gives the Damkohler number Da_x shown in Fig. 6b. Based on a transition Reynolds number of 2×10^4 we estimate x_t = 13.6 cm for the U_1 = 22 m/s case and x_t = 6.8 cm for the U_1 = 44 m/s case, so that the mixing times are 20.8 msec and 12.6 msec respectively. Based on this criterion, the mixing limited (fast chemistry) regime occurs past $Da_x \sim 40$. Finite rate effects occur below this value with a symmetric profile occuring for $Da_x \sim 4$.

Alternately, one may choose the local large scale turnover time to be the mixing time $(\delta_1/\Delta U)$ to define a different Damkohler number, Da_1. By this definition, Da_1 varies from 0.8 to 17 for the range of [NO] investigated. This suggests that past $Da_1 \sim 10$, the reaction is mixing limited while for $Da_1 \sim 1$, the reaction profile is symmetric. Wallace [15] for a nitric oxide - ozone mixing layer was able to achieve $1 < Da_1 < 16$ at high Reynolds number, while Masutani [16] achieved $2 < Da_1 < 28$ at pre-transitional Reynolds numbers using the same chemical system as Wallace. A further discussion of Fig. 6b will be made in Broadwell & Mungal [7] when a detailed comparison of the results are made with the model.

Figures. 7a, 7b show sample temperature vs time traces obtained from the eight cold wires at U_1 = 22 m/s, for $[NO]/[NO]^*$ = 1 and 1/32, i.e. for fast and slow chemistry. The time traces show the instantaneous temperature rise recorded by each probe as a function of time, normalized by the highest temperature rise of any probe during this time interval (labeled Tmax). The vertical distance between a consecutive pair of horizontal axes therefore represents Tmax. The horizontal axis corresponds to 51.2 ms of real time. Flow can be viewed as being from right to left with the high-speed fluid at the top. The time axis is greatly compressed in the sense that such a plot would be to geometric scale only if the

horizontal distance were about nine times the distance between the high-speed and low-speed probes.

We have discussed such traces in [1,2,4] and noted the presence of large regions of high temperature, associated with the large scale structure, separated by tongues of unreacted, cool gas. Here however, we wish to discuss the ramp-like temperature traces shaded in Fig. 7a, the data for the high kinetic rate, and, to point out that they are not present when the rate is slow, Fig. 7b.

If one pictures a large structure undergoing reaction, then for the present choice of reactant concentrations, the large structure is hydrogen rich. The effect of free-stream addition of fluid to the structure is to create a situation whereby the composition of the upper and downstream edges of the structure is biased toward the high-speed fluid, while the composition of the upstream and lower edges are biased toward the low-speed, lean reactant fluid. This leads to lateral (y) and axial (x) gradients in composition, and hence in temperature. In the fast chemistry case the consequences are the ramp-like structures and time traces which on the lean reactant edge reach generally higher instantaneous temperatures than those of the rich reactant edge. The skewed mean temperature profiles as shown in Fig. 3b result from long time averages of such traces. These features are to be contrasted with the time traces of Fig. 7b, for a slow reaction rate. Here the ramp-like features are much less apparent (become more top-hat) and the time traces of all probes generally reach the same maximum instantaneous temperatures from one edge of the layer to the other. The long time average of such traces leads to the symmetric mean temperature profiles of Fig. 3a. We note that ramps do not occur for every structure in the fast-chemistry limit but tend to be observed more often than not. Similarly, ramps are sometimes present when the reaction rate is low, but their occurance is quite infrequent.

We also note that since the fluid mechanics is unaffected by these low values of heat release, the instantaneous mixture fraction distribution of high-speed to low-speed fluid in the mixing layer is similar for the fast and slow chemistry cases. In the fast chemistry limit, the instantaneous mixture fraction uniquely determines the temperature at every point in the layer (see Bilger [17] and [2]). For lower reaction rates, this is no longer true - the temperature at any given point being determined by its history. We also note that the two main features of the slow chemistry results discussed above - namely, a symmetric mean temperature profile and the lack of ramp-like structures are in agreement with the measurements of Koochesfahani [3] in a chemically reacting liquid mixing layer, in the limit of fast chemistry, at comparable Reynolds numbers. The connection between these seemingly unrelated observations (slow chemistry in gases and fast chemistry in liquids) and a further discussion of these results appear in Broadwell & Mungal [7].

6. Conclusions

The experiments discussed above describe the behavior of the product field in a two-dimensional, turbulent mixing layer as the overall chemical rate is varied while the fluid mechanics and the heat of reaction remain unchanged. As we proceed from the mixing limited regime to the chemical rate limited regime, three main effects are observed: (1) the amount of product declines, (2) the mean-temperature profile, which is initially somewhat unsymmetrical because of the large hydrogen-fluorine reactant concentration ratio, becomes symmetrical, and (3) the ramp-like instantaneous temperature traces within the large structures become more top-hat. At the mixing limited (fast chemistry) regime, the Damkohler number based on time of flight from the mixing transition exceeds about 40. Below this value we enter the rate limited regime with a symmetric profile attained at a Damkohler number of about 4 (based on the local large scale turnover time, the Damkohler numbers become 10 and 1 respectively). Detailed comparison of these results with a theoretical model is presented

in Broadwell & Mungal [7].

7. Acknowledgments

The authors wish to thank Dr. J. E. Broadwell (who is an unofficial co-author) for numerous technical discussions, Dr. P. E. Dimotakis, Dr. W. L. Shackleford, Dr. R. C. Miake-Lye and Mr. Earl Dahl for help in conducting the experiments. This work is sponsored by the Air Force Office of Scientific Research under Grant No. 83-0213.

Table 1 - Summary of Results, U_1 = 22 m/s.

$\frac{[NO]}{[NO]^*}$	$\frac{\delta_1}{(x-x_0)}$	$\frac{\bar{T}max}{Tflm}$	A	$\frac{\delta_p}{\delta_1}$	$\frac{k}{k^*}$
2	0.170	0.540	0.0457	0.251	1.53
3/2	0.163	0.531	0.0419	0.231	1.29
1	0.165	0.537	0.0436	0.240	1.00
1/2	0.171	0.511	0.0429	0.236	1/1.49
1/4	0.165	0.488	0.0408	0.225	1/2.37
1/8	0.165	0.443	0.0365	0.201	1/3.98
1/16	0.165	0.396	0.0330	0.182	1/6.80
1/23	0.169	0.253	0.0220	0.121	1/9.11
1/32	0.168	0.197	0.0169	0.093	1/12.2
0	-	0	0	0	0

Table 2 - Summary of Results, U_1 = 44 m/s.

$\frac{[NO]}{[NO]^*}$	$\frac{\delta_1}{(x-x_0)}$	$\frac{\bar{T}max}{Tflm}$	A	$\frac{\delta_p}{\delta_1}$	$\frac{k}{k^*}$
2	0.165	0.491	0.0405	0.223	1.53
1	0.163	0.475	0.0391	0.215	1.00
1/4	0.169	0.433	0.0364	0.200	1/2.37
1/16	0.168	0.301	0.0264	0.145	1/6.80
0	-	0	0	0	0

Tflm ≡ adiabatic flame-temperature rise = 158.7K; Tmax ≡ maximum value of T; δ_1 ≡ width of layer where $\bar{T}$ = 1% of Tmax; $A \equiv \frac{1}{Tflm}\int \bar{T} d\eta$; $\eta \equiv \frac{y}{(x-x_0)}$; A^* = nominal condition at 22 m/s; $(x-x_0)$ = 45.7 cm for all runs; $k = 1/\tau$ = overall chemical rate; τ = chemical time determined from CHEMKIN.

Table 3 - Curvefit constants, U_1 = 22 m/s, $\tilde{y}_o$ = -.35

$\frac{[NO]}{[NO]^*}$	c_o	c_1	c_2	c_3	c_4
2	4.0596	-0.9089	-0.5342	-0.4929	-0.6328
3/2	3.9804	-0.1009	-0.4528	-0.4400	-0.7601
1	4.0568	-0.9833	-0.5925	-0.4336	-0.6720
1/2	4.0402	-0.9582	-0.6372	-0.3622	-0.5524
1/4	4.0497	-0.8729	-0.6610	-0.4596	-0.6561
1/8	3.9407	-0.9110	-0.6674	-0.4094	-0.6425
1/16	3.9311	-0.8084	-0.8073	-0.3656	-0.5957
1/23	3.5560	-0.6492	-0.8642	-0.4248	-0.5362
1/32	3.3329	-0.5917	-0.8614	-0.3242	-0.5277
0	0	0	0	0	0

Table 4 - Curvefit Constants, U_1 = 44 m/s, $\tilde{y}_o$ = - .32

$\frac{[NO]}{[NO]^*}$	c_o	c_1	c_2	c_3	c_4
2	4.1344	-0.8340	-0.7880	-0.3105	-0.5942
1	4.1159	-0.8224	-0.8642	-0.3837	-0.6047
1/4	4.0793	-0.7320	-0.9205	-0.2822	-0.4830
1/16	3.7876	-0.4951	-0.8463	-0.4140	-0.5587
0	0	0	0	0	0

Mean Temperature Rise, T (°K) recorded in physical coordinates, $\tilde{y}$ (inches) where

$$T(\tilde{y}) = \exp\left(c_o + c_1\tilde{y} + c_2\tilde{y}^2 + c_3\tilde{y}^3 + c_4\tilde{y}^4\right)$$

$-3 < \tilde{y} < 2$, $\eta \equiv (\tilde{y}-\tilde{y}_o)/(x-x_o)$ and $(x-x_o)$ = 18.0 in. for all runs.

Appendix 1

The ideas in this section were developed by J.E. Broadwell to provide a simple understanding of how the NO concentration controls the overall reaction rate.

It was shown above that reactions (1)-(3) can be considered as being representative of the H_2-F_2-NO chemistry, since the addition of reactions (4)-(7) showed essentially no change in the behaviour of the system as seen from Fig. 2. It is possible to estimate the overall behaviour of the system by the following arguments. From (2), (3)

$$\frac{dF_2}{dt} = -k_2HF_2 - k_3NOF_2 \tag{9}$$

$$\frac{dNO}{dt} = -k_3NOF_2 \tag{10}$$

This represents two equations for the three unknowns F_2, NO, H. By using either the rate equations or conservation of atoms it is possible to show that

$$H + F + NO = \text{const} = NO_i \tag{11}$$

since the initial concentrations (subscript i) of H and F are zero. Examination of (1)-(3) together with the fact that $k_1 > k_2 >> k_3$ would suggest that any F atoms produced (slowly) in (2), (3) would be (quickly) depleted in (1), hence a reasonable approximation would be to take $F \tilde{} 0$. This approximation now simplifies (11) to $H = NO_i - NO$ which can be substituted into (9), (10) to yield

$$\frac{dF_2}{dt} = -k_2NO_iF_2 + (k_2 - k_3)NOF_2 \tilde{} -k_2NO_iF_2 + k_2NOF_2 \tag{12}$$

$$\frac{dNO}{dt} = -k_3 NO F_2 \qquad (13)$$

the system now being reduced to two equations in the two unknowns F_2 and NO.

In order to proceed further, the CHEMKIN simulations were used as a guide as they suggested two types of behaviour. In the first case, for small NO concentrations, CHEMKIN suggested that the NO would deplete while the F_2 concentration had remained relatively fixed. Thus, if we assume $F_2 \sim F_{2i}$ we solve (13) which yields $NO/NO_i = e^{-k_3 F_{2i} t}$ and substituting into (12) gives

$$\frac{dF_2}{dt} = -k_2 NO_i F_2 (1-e^{-k_3 F_{2i} t})$$

or

$$\frac{dF_2}{d\tau} = -F_2 (1-e^{-\frac{k_3 F_{2i}}{k_2 NO_i}\tau})$$

where $\tau = k_2 NO_i t$. The second term can be neglected for $NO_i << \frac{k_3}{k_2} F_{2i}$ to yield the approximate solution

$$\frac{F_2}{F_{2i}} = e^{-k_2 NO_i t}.$$

Thus for $NO_i << \frac{k_3}{k_2} F_{2i}$, the overall rate will be proportional to NO_i.

The second case suggested by CHEMKIN concerns large NO concentrations for which the amount of NO changed slightly but did not deplete during the times of interest. We therefore take $NO \sim NO_i$ in (13). To solve, we further assume in (13) that $F_2 \sim F_{2i}$. This yields the solution $NO/NO_i = 1-k_3 F_{2i} t$ (This expression would imply negative NO concentrations

for long time and must of course be valid for times $t << 1/k_3F_{2i}$. Alternately we might interpret this as the leading term in an expansion for the NO behaviour). With this expression, (12) becomes

$$\frac{dF_2}{dt} = -k_2k_3NO_iF_{2i}F_2t$$

with solution

$$\frac{F_2}{F_{2i}} = e^{-k_2k_3NO_iF_{2i}t^2/2} \qquad (15)$$

Thus for large NO concentrations, the overall rate is now proportional to $NO^{1/2}$. The overall reaction rate derived from the CHEMKIN simulations is shown in Fig. 8 as a function of NO concentration. The initial linear trend followed by the square root behaviour seems consistent with the preceeding analysis.

The arguments above suggest that the overall rate varies linearly with NO, for small NO, and then as the square root of NO for larger values of NO. This of course is a complication and raises the question of whether a single overall rate can be found for each run condition that accurately describes the behaviour of the system. Using the linear extrapolation technique shown Fig. 2 for each case yields a characteristic time, τ (see last column of Table 1). The CHEMKIN results for all cases using reactions (1)-(7) are shown in Fig. 9, where the abscissa has been scaled by the appropriate characteristic time. The similarity of shape for all curves suggests that choosing a single overall rate seems reasonable for describing the reaction set.

Appendix 2

For the record we include the following curvefit constants for the runs reported in References 2,4. The same notation as Tables 3,4 is used, and $(x-x_o) = 18.0$ for all runs.

Table 5 - Curvefit Constants of Reference 2, Table 1

ϕ	T_{flm}	c_o	c_1	c_2	c_3	c_4	$\tilde{y}_o$
1/8	165	4.2985	-0.7807	-0.6762	-0.0573	-0.5953	-0.175
1/4	149	4.2841	-0.6418	-0.8488	-0.0483	-0.5209	-0.175
1/2	124	4.2454	-0.5327	-0.9712	-0.0772	-0.4759	-0.175
1	93	4.0740	-0.1913	-1.0964	-0.2538	-0.3959	-0.175
1	93	3.9809	-0.7483	-1.2209	-0.6152	-0.4835	-0.425
2	124	4.3743	-0.5202	-1.5259	-0.9914	-0.5786	-0.425
4	149	4.5414	-0.3831	-1.6016	-1.1379	-0.5972	-0.425
8	165	4.6320	-0.2451	-1.7962	-1.4960	-0.7309	-0.425

Table 6 - Curvefit Constants of Reference 2, Table 2

ϕ	T_{flm}	c_o	c_1	c_2	c_3	c_4	$\tilde{y}_o$
1/2	137.5	3.9154	-1.0811	-0.9082	0.8426	-0.6098	+0.300
1	109.0	3.8242	-0.9398	-1.0662	0.5143	-0.3058	+0.300
2	154.0	4.3746	-0.7190	-0.8895	0.3105	-0.4022	+0.300

Table 7 - Curvefit Contants of Reference 4

Run	c_o	c_1	c_2	c_3	c_4	$\tilde{y}_o$
Re_1	4.1019	-0.7526	-0.5933	-0.5687	-0.6048	-0.325
Re_2	4.1603	-0.9880	-0.9188	-0.5182	-0.6362	-0.325
Re_3	4.1105	-0.7930	-0.9572	-0.6126	-0.6033	-0.325
Re_{2T}	4.0359	-1.7096	-1.1633	-1.0232	-3.4653	-0.210
Re_{3T}	4.0223	-1.7280	-2.0311	-0.7710	-1.9014	-0.210
Re_4	3.9053	-1.7094	-1.5894	-0.8499	-1.9001	-0.210

8. References

[1] MUNGAL, M.G., DIMOTAKIS, P.E. & BROADWELL, J.E. 1984 Turbulent Mixing and Combustion in a Reacting Shear Layer. AIAA Jr., 22 (6), 797-800.

[2] MUNGAL, M.G. & DIMOTAKIS, P.E. 1984 Mixing and Combustion with Low Heat Release in a Turbulent Shear Layer. J. Fluid Mech., 148, 349-382.

[3] KOOCHESFAHANI, M.M. 1984 Experiments on Turbulent Mixing and Chemical Reactions in a Liquid Mixing Layer. Ph.D. Thesis, Caltech.

[4] MUNGAL, M.G., HERMANSON, J.C. & DIMOTAKIS P.E. 1985 Reynolds Number Effects on Mixing and Combustion in a Reacting Shear Layer. AIAA Jr. 23 (9), 1418-1423.

[5] KEE, R.J., MILLER, J.A. & JEFFERSON, T.H. 1980 CHEMKIN: A General-Purpose, Problem-Independent, Transportable, Fortran Chemical Kinetics Code Package. SANDIA Report SAND80-8003.

[6] BROADWELL, J.E. & BREIDENTHAL, R.E. 1982 A Simple Model of Mixing and Chemical Reaction in a Turbulent Shear Layer. J. Fluid Mech., 125, 397-410.

[7] BROADWELL, J.E. & MUNGAL, M.G. 1986 The Effects of Damkohler Number on a Turbulent Shear Layer - Analysis. Submitted to 21st (Intl.) Symp. on Combustion, The Combustion Institute.

[8] COHEN, N. & BOTT, J.F. 1982 Review of Rate Data for Reactions of Interest in HF and DF Lasers. The Aerospace Corporation, Report SD-TR-82-86.

[9] BAULCH, D.L., DUXBURY, J., GRANT, S.J., MONTAGUE, D.C. 1981 Evaluated Kinetic Data for High Temperature Reactions, Vol. 4, J. Phys. Chem. Ref. Data, Vol. 10, Suppl. 1.

[10] KONRAD, J.H. 1976 An Experimental Investigation of Mixing in Two-Dimensional Turbulent Shear Flows with Application to Diffusion-Limited Chemical Reactions. Ph.D. Thesis, Caltech, and Project SQUID Technical Report CIT-8-PU.

[11] BREIDENTHAL, R.E. 1981 Structure in Turbulent Mixing Layers and Wakes using a Chemical Reaction. J.Fluid Mech., 109, 1-24.

[12] BETCHOV, R. 1948 Proc. Ned. Akad. Wetenshappen, 51, 721.

[13] PARANTHOEN, P., PETIT, C. & LECORDIER, J.C. 1982 The Effect of the Thermal Prong - Wire Interaction on the Response of a Cold Wire in Gaseous Flows (Air, Argon and Helium), J. Fluid Mech., 124, 457-473.

[14] SCADRON, M.D. & WARSHAWSKY, I. 1952 Experimental Determination of Time Constants and Nusselt Numbers for Bare-Wire Thermocouples in High-Velocity Air Streams and Analytic Approximation of Conduction and Radiation Errors, NACA TN 2599.

[15] WALLACE, A.K. 1981 Experimental Investigation of the Effects of Chemical Heat Release in the Reacting Turbulent Plane Shear Layer, Ph.D. Thesis, The University of Adelaide; also AFOSR Report AFOSR-TR-84-0650.

[16] MASUTANI, S.M. 1985 An Experimental Investigation of Mixing and Chemical Reaction in a Plane Mixing Layer, Ph.D. Thesis, Stanford University.

[17] BILGER, R.W. 1980 Turbulent Flows with Nonpremixed Reactants, in Turbulent Reacting Flows, Topics in Applied Physics, 44, Springer-Verlag.

9. Figure Captions

Fig. 1 Turbulent Shear Layer Geometry.

Fig. 2 CHEMKIN Simulation of Constant Pressure Reactor using Reactions (1)-(3) and (1)-(7). $[NO]/[NO]^* = 1$.

Fig. 3a Normalized Mean Temperature Profiles for decreasing [NO], U_1 = 22 m/s. $[NO]/[NO]^*$: □ - 1, ○ - 1/2, △ - 1/4, + - 1/8, × - 1/16, ▽ - 1/23, ◇ - 1/32, ◆ - 0.

Fig. 3b Scaled Mean Temperature Profiles for decreasing [NO], U_1 = 22 m/s. Symbols same as Fig. 3a.

Fig. 3c Scaled Mean Temperature Profiles for $[NO]/[NO]^*$ = 1 & 1/32, U_1 = 22 m/s. Symbols same as Fig. 3a.

Fig. 4 Normalized Mean Temperature Profiles for increasing [NO], U_1 = 22 m/s. $[NO]/[NO]^*$: □ - 1, ○ - 3/2, △ - 2.

Fig. 5a Normalized Mean Temperature Profiles for varying [NO], U_1 = 44 m/s. $[NO]/[NO]^*$: □ - 1, ○ - 1/4, △ - 1/16, + -2.

Fig. 5b Scaled Mean Temperature Profiles for $[NO]/[NO]^*$ = 1 & 1/16, U_1 = 44 m/s. Symbols same as Fig. 5a.

Fig. 6a Normalized Product Thickness vs Nitric Oxide Concentration.

Fig. 6b Normalized Product Thickness vs Time of Flight Damkohler Number.

Fig. 7a Temperature vs Time Trace, $[NO]/[NO]^* = 1$, U_1 = 22 m/s.

Fig. 7b Temperature vs Time Trace, $[NO]/[NO]^* = 1/32$, U_1 = 22 m/s.

Fig. 8 k/k^* vs $[NO]/[NO]^*$ from CHEMKIN simulations for Reactions (1)-(7).

Fig. 9 CHEMKIN Simulations of Constant Pressure Reactor using Reactions (1)-(7) for [NO] shown in Table 1.

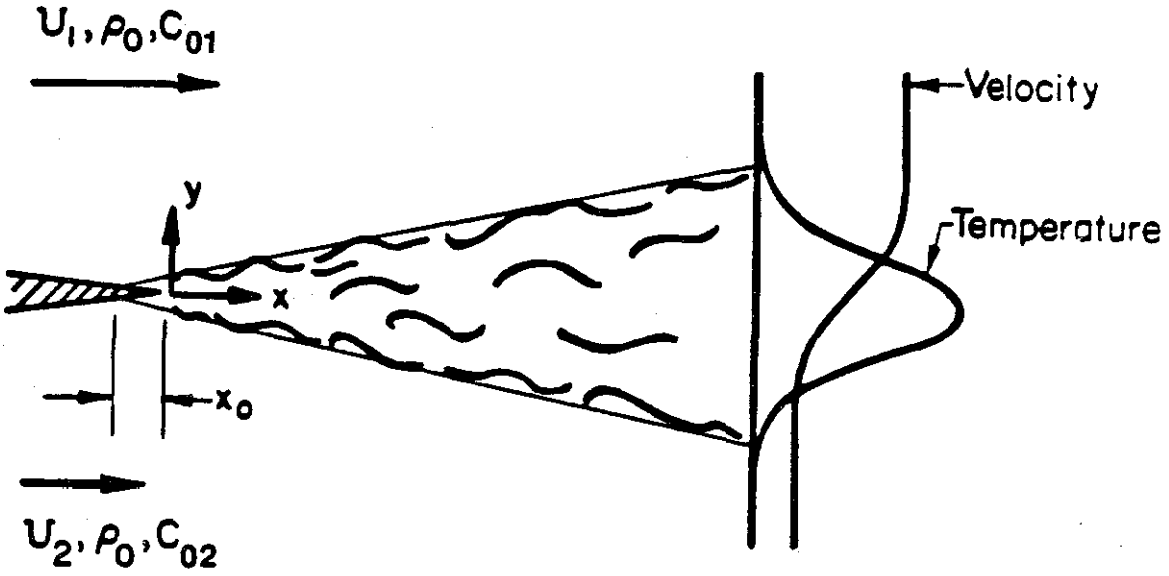

1

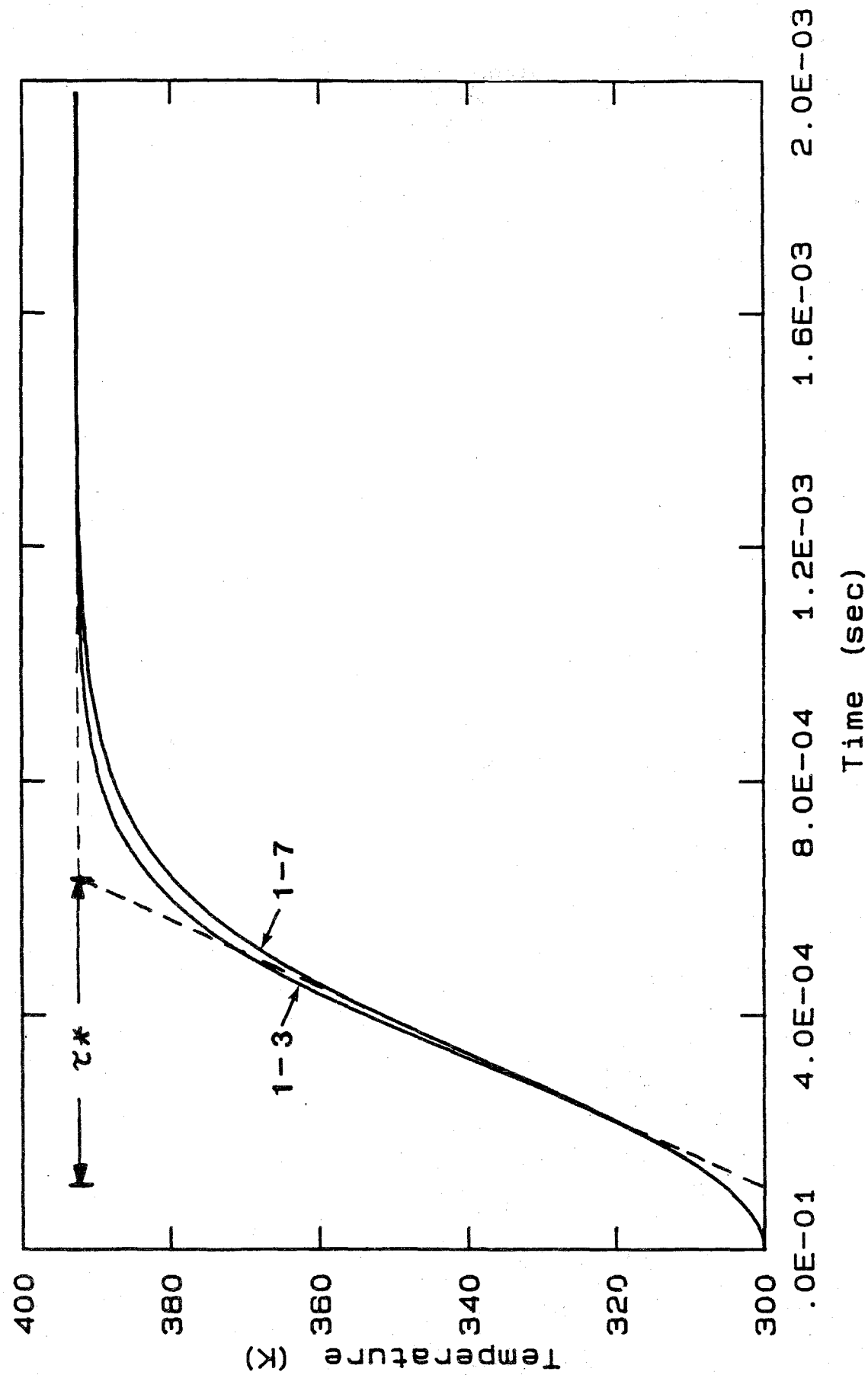
400
380
360
340
320
300
Temperature (K)
.0E-01
4.0E-04
8.0E-04
1.2E-03
1.6E-03
2.0E-03
Time (sec)
τ*
1-7
1-3

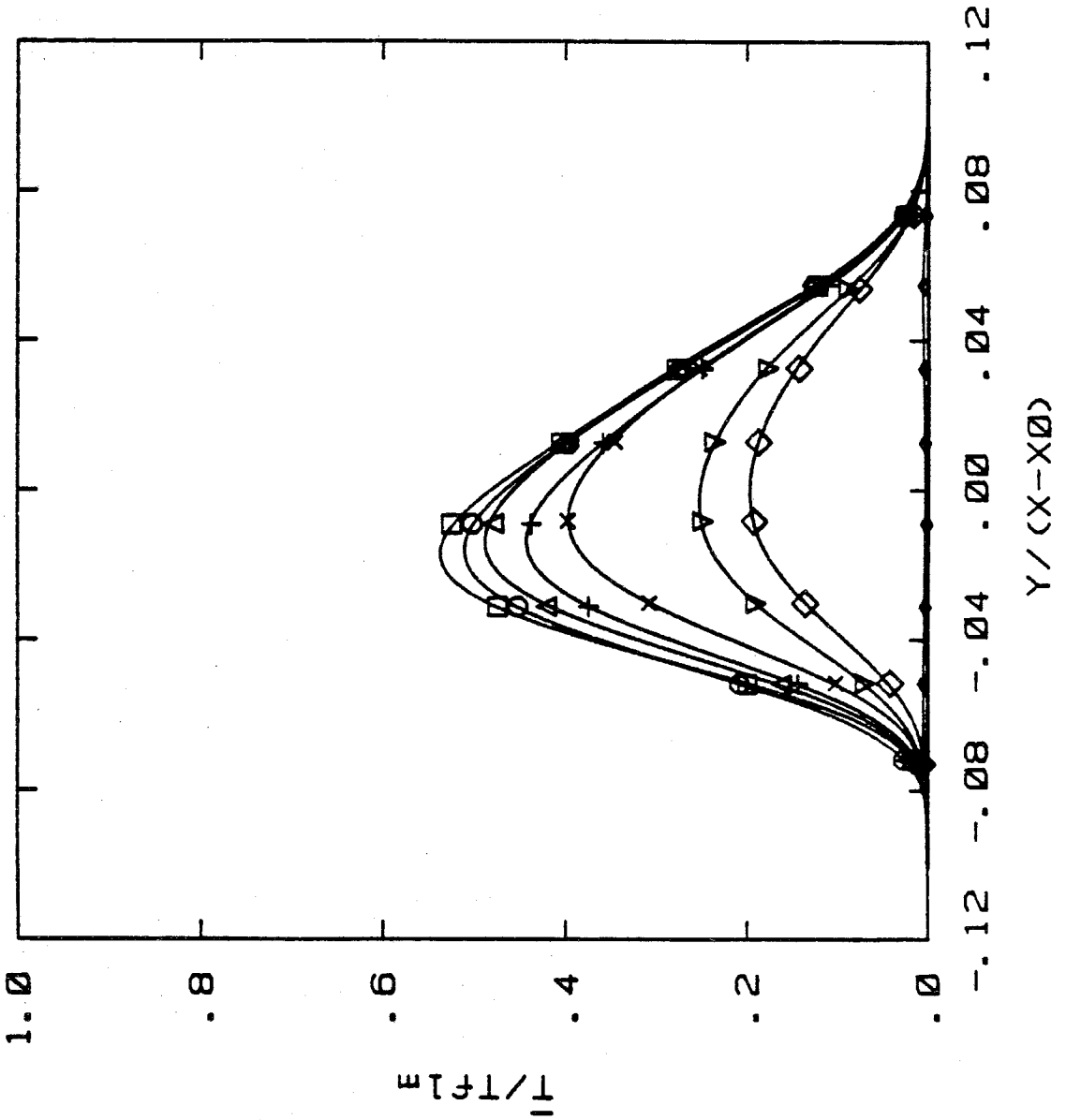
1.0
.8
.6
.4
.2
0
$\overline{T}/Tf1_\infty$
-.12
-.08
-.04
.00
.04
.08
.12
Y/(X-X0)

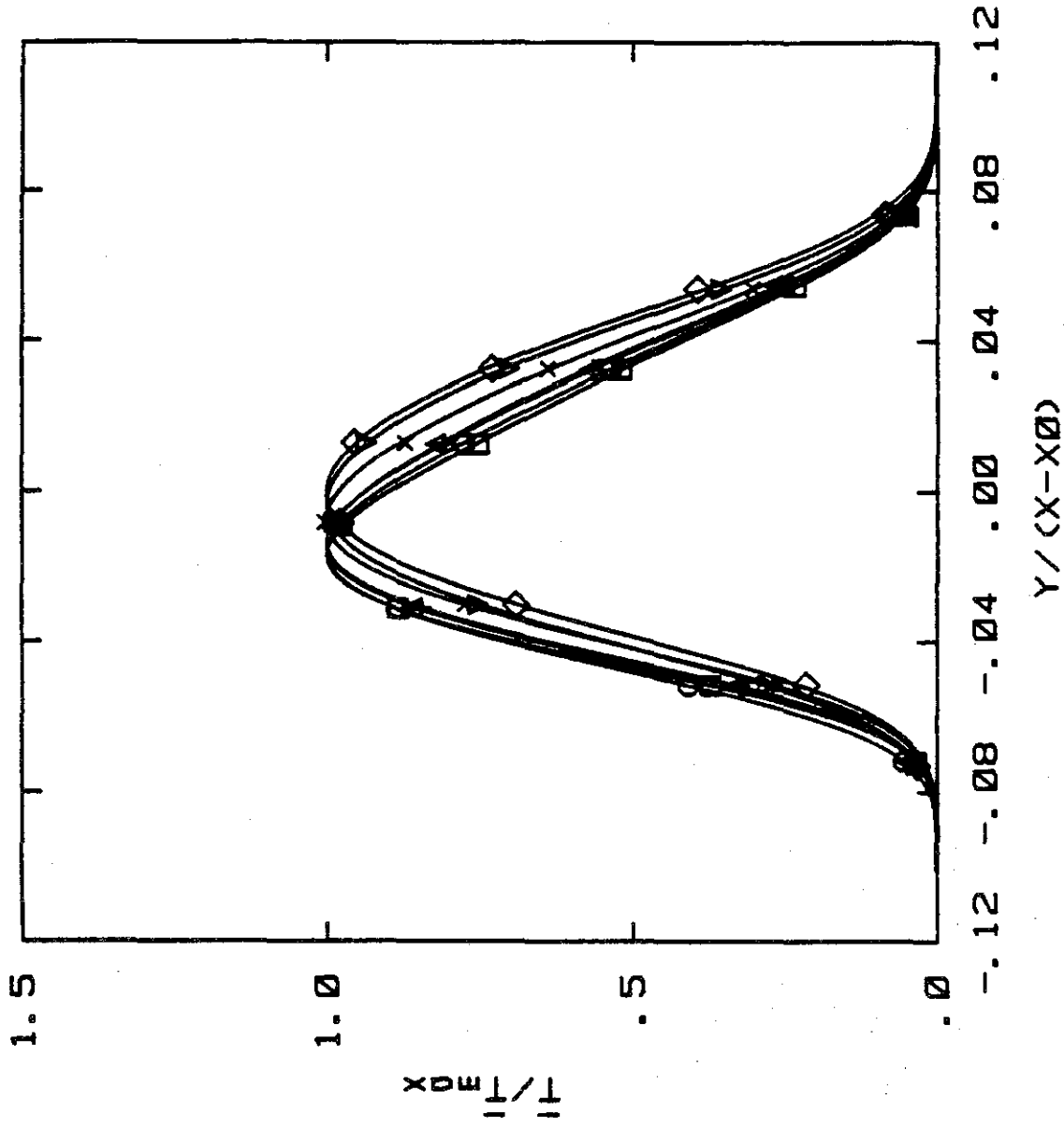
1.5
1.0
.5
.0
$\overline{T}/\overline{T}_{max}$
-.12
-.08
-.04
.00
.04
.08
.12
Y/(X-X0)

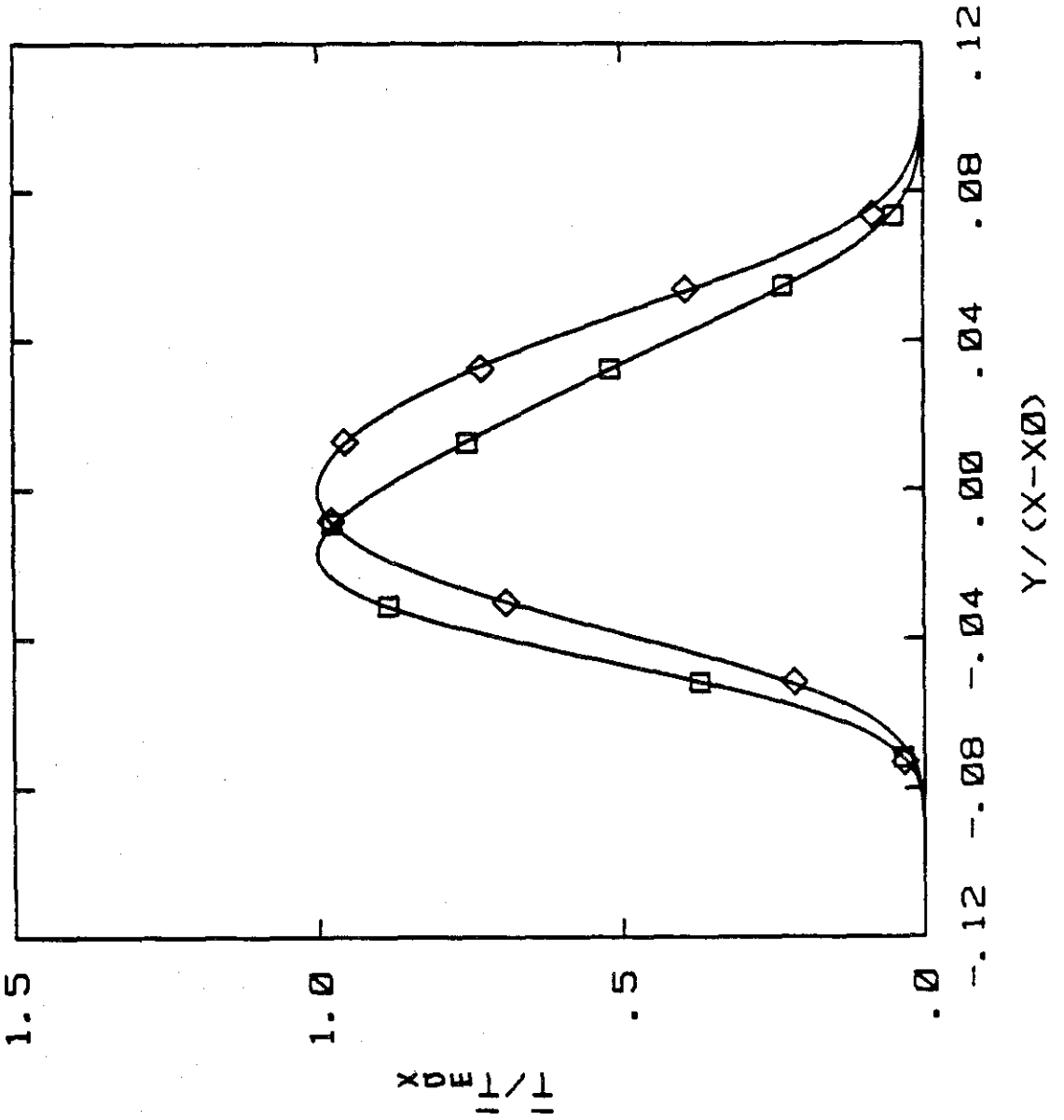
1.5
1.0
.5
.0
T/Tmax
-.12
-.08
-.04
.00
.04
.08
.12
Y/(X-X0)

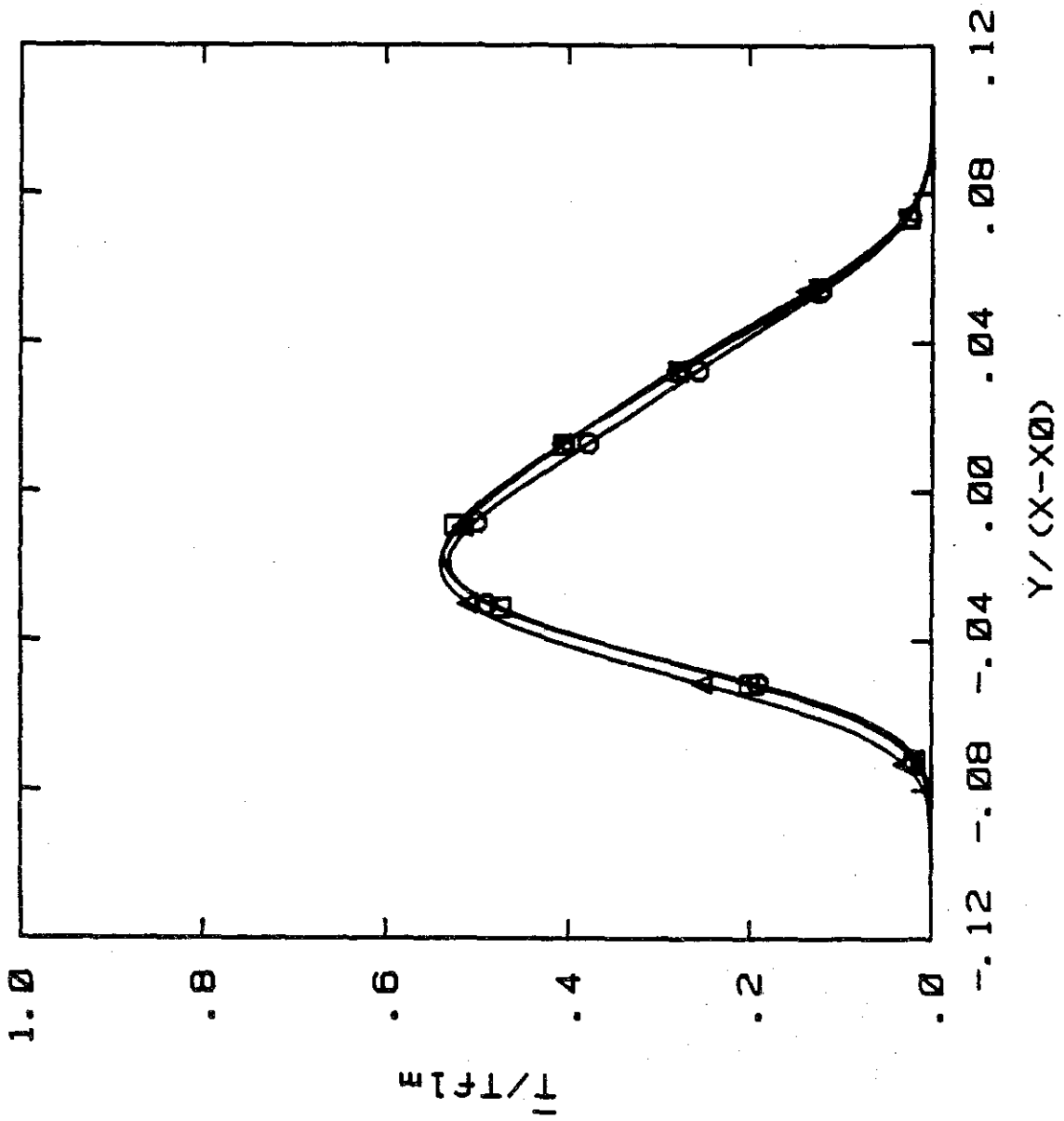
1.0
.8
.6
.4
.2
.0
T/TFlm
-.12
-.08
-.04
.00
.04
.08
.12
Y/(X-X0)

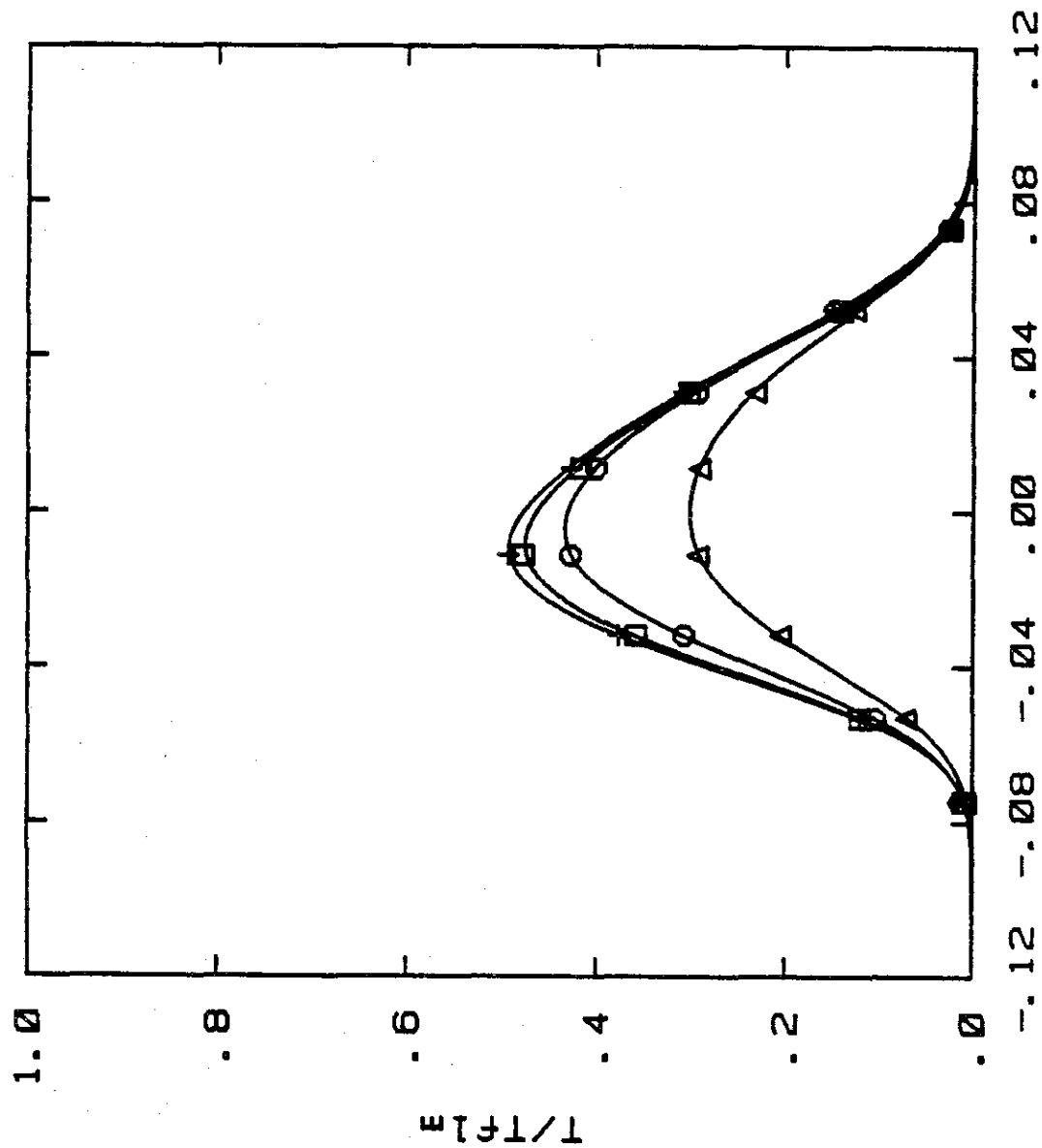

5a

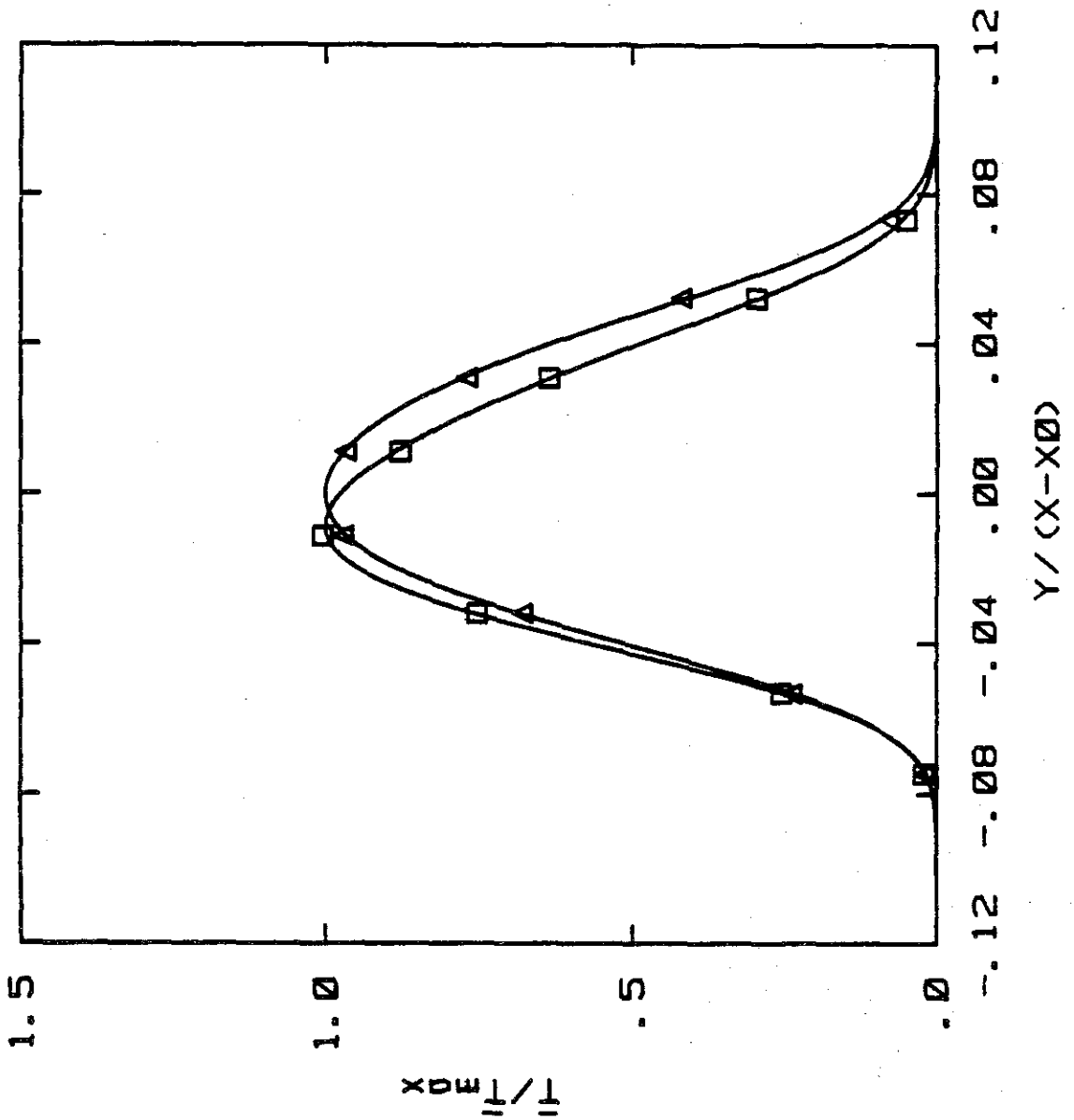

5b

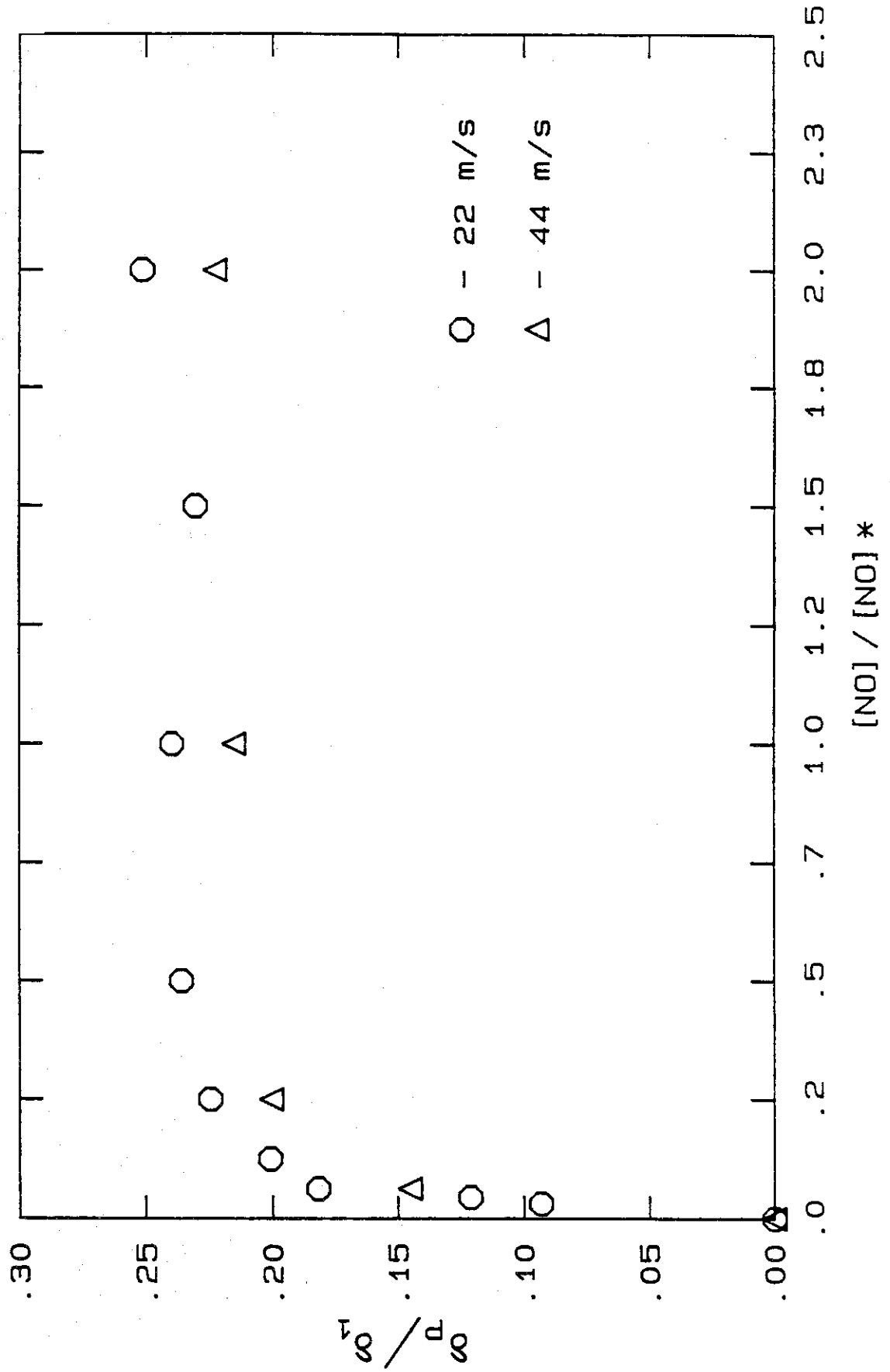
.30
.25
.20
.15
.10
.05
.00
δ_p / δ_1
.0
.2
.5
.7
1.0
1.2
1.5
1.8
2.0
2.3
2.5
[NO] / [NO] *
○ - 22 m/s
△ - 44 m/s

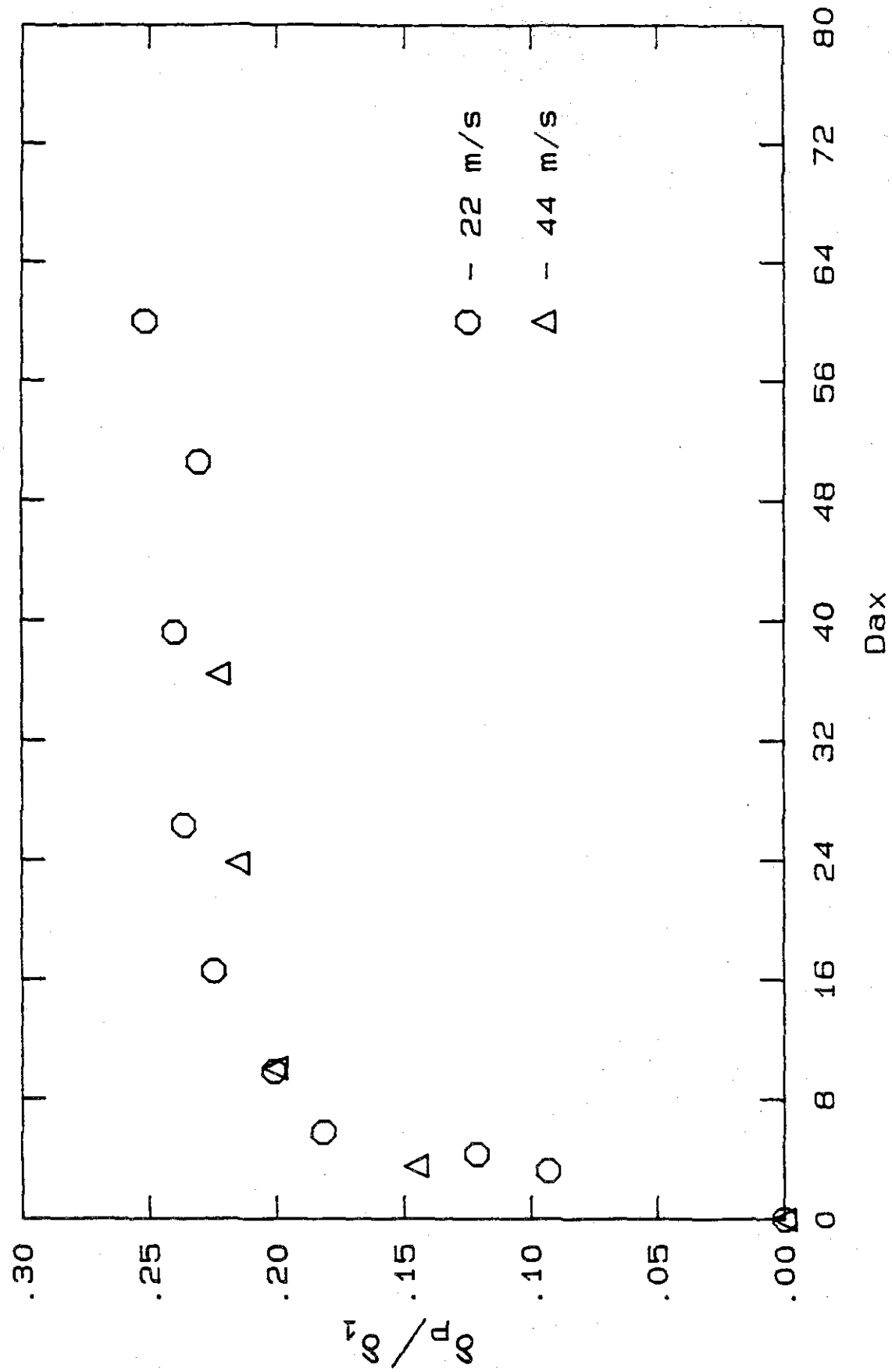
○ - 22 m/s
△ - 44 m/s
δ_p / δ_1
Dax
.30
.25
.20
.15
.10
.05
.00
0
8
16
24
32
40
48
56
64
72
80

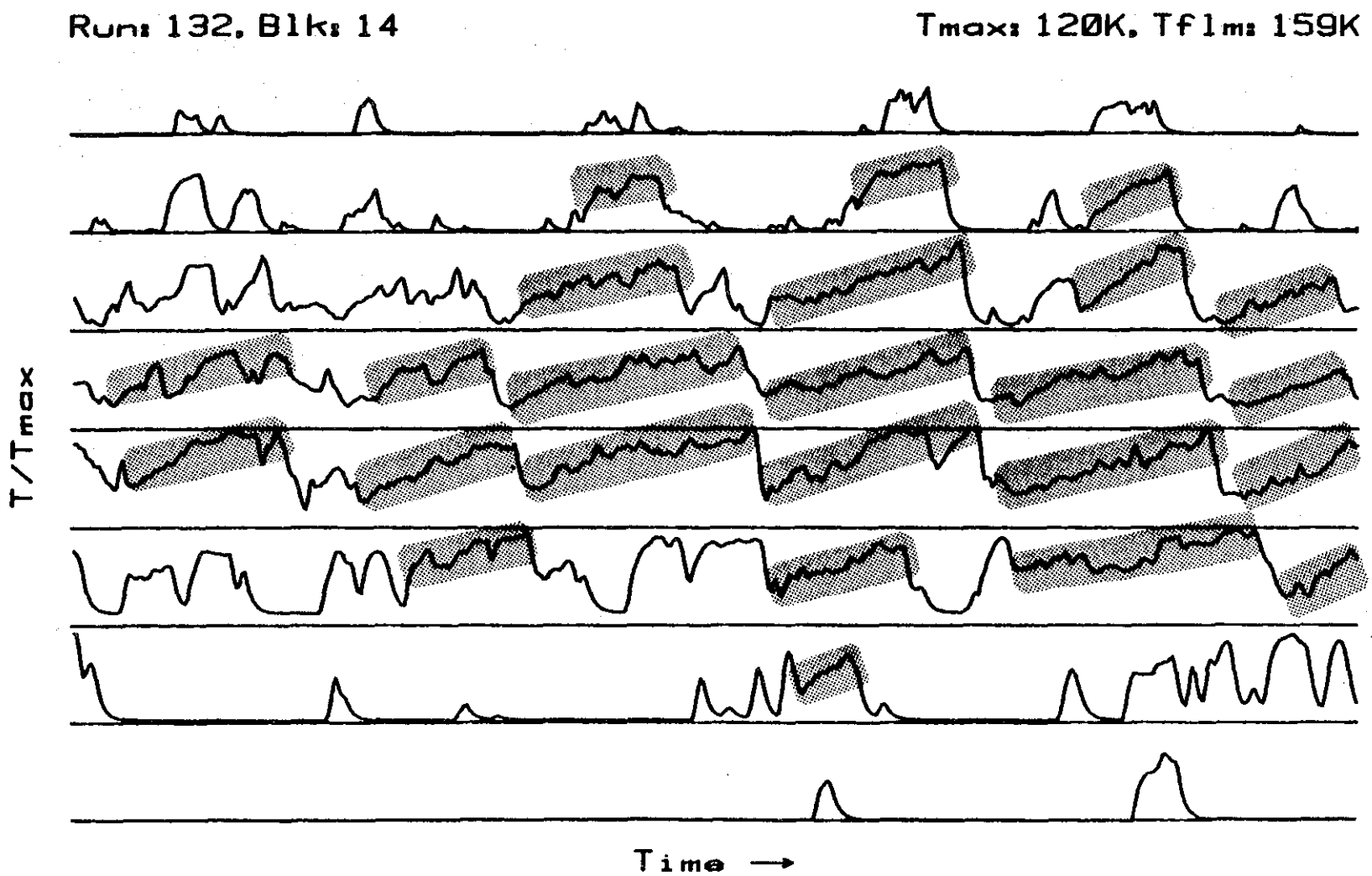

7a

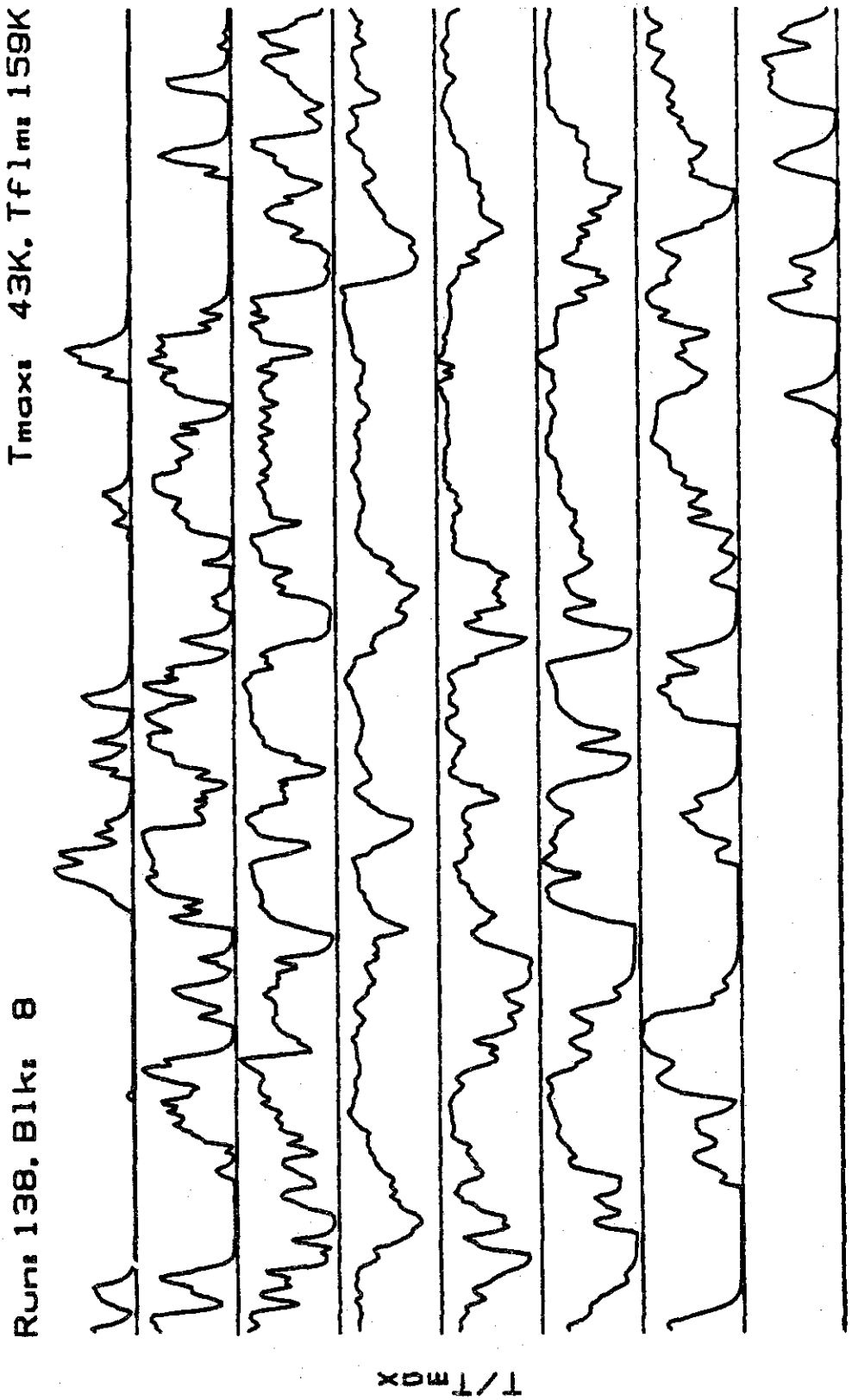
Run: 138, Blk: 8
Tmax: 43K, Tfilm: 159K
T/Tmax
Time →

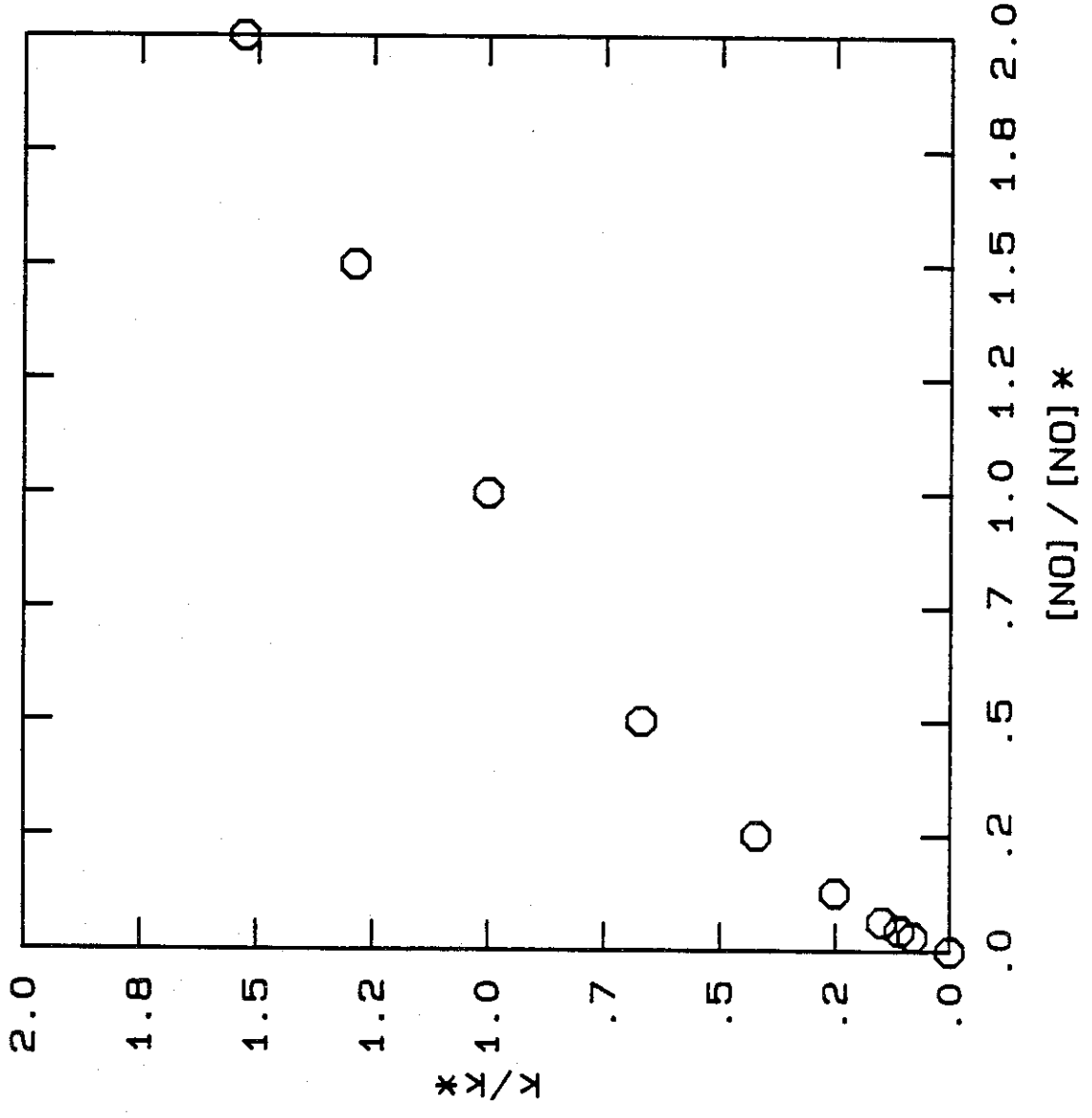
k/k*
2.0
1.8
1.5
1.2
1.0
.7
.5
.2
.0
.0
.2
.5
.7
1.0
1.2
1.5
1.8
2.0
[NO] / [NO] *

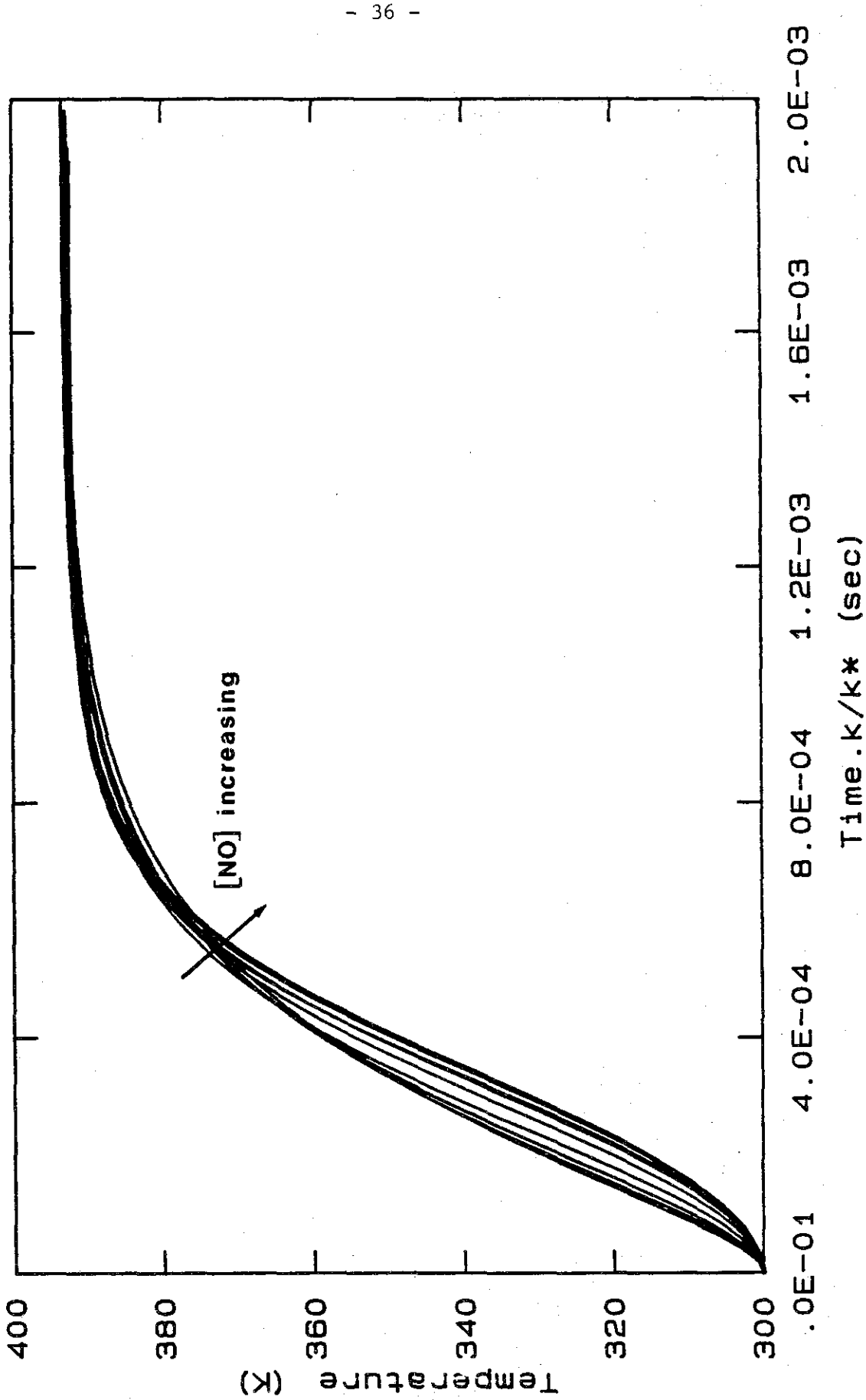
Temperature (K)
400
380
360
340
320
300
.0E-01
4.0E-04
8.0E-04
1.2E-03
1.6E-03
2.0E-03
Time.k/k* (sec)
[NO] increasing